Quantifying Defects in Graphene via Raman Spectroscopy at Different Excitation Energies

L. G. Cançado,[*,†] A. Jorio,[†] E. H. Martins Ferreira,[‡] F. Stavale,[‡] C. A. Achete,[‡] R. B. Capaz,[§] M. V. O. Moutinho,[§] A. Lombardo,[‖] T. S. Kulmala,[‖] and A. C. Ferrari[‖]

[†]Departamento de Física, Universidade Federal de Minas Gerais, 30123-970, Belo Horizonte, Brazil

[‡]Divisão de Metrologia de Materiais, Instituto Nacional de Metrologia, Normalização e Qualidade Industrial (INMETRO), 25250-020, Brazil

[§]Instituto de Física, Universidade Federal do Rio de Janeiro, 21941-972, Brazil

[‖]Department of Engineering, University of Cambridge, Cambridge CB3 0FA, United Kingdom

ABSTRACT: We present a Raman study of Ar^+-bombarded graphene samples with increasing ion doses. This allows us to have a controlled, increasing, amount of defects. We find that the ratio between the D and G peak intensities, for a given defect density, strongly depends on the laser excitation energy. We quantify this effect and present a simple equation for the determination of the point defect density in graphene via Raman spectroscopy for any visible excitation energy. We note that, for all excitations, the D to G intensity ratio reaches a maximum for an interdefect distance ~3 nm. Thus, a given ratio

could correspond to two different defect densities, above or below the maximum. The analysis of the G peak width and its dispersion with excitation energy solves this ambiguity.
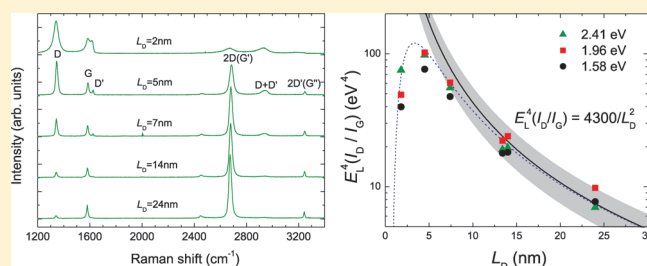
KEYWORDS: Graphene, defects, Raman spectroscopy, excitation energy

Quantifying defects in graphene related systems, which include a large family of sp^2 carbon structures, is crucial both to gain insight in their fundamental properties and for applications. In graphene this is a key step toward the understanding of the limits to its ultimate mobility.[1−3] Significant efforts have been devoted to quantify defects and disorder using Raman spectroscopy for nanographites,[4−20] amorphous carbons,[18−24] carbon nanotubes,[25,26] and graphene.[11,27−35] The first attempt was the pioneering work of Tuinstra and Koenig.[4] They reported the Raman spectrum of graphite and nanocrystalline graphite and assigned the mode at ~1580 cm^{-1} to the high frequency E_{2g} Raman allowed optical phonon, now known as G peak.[5] In defective and nanocrystalline samples they measured a second peak at ~1350 cm^{-1}, now known as D peak.[5] They assigned it to an A_{1g} breathing mode at the Brillouin Zone (BZ) boundary **K**, activated by the relaxation of the Raman fundamental selection rule **q** ≈ 0, where **q** is the phonon wavevector.[4] They noted that the ratio of the D to G intensities varied inversely with the crystallite size, L_a. Reference 18 noted the failure of the Tuinstra and Koenig relation for high defect densities and proposed a more complete amorphization trajectory valid to date. References 7, 8, 18, and 19 reported a significant laser excitation energy, E_L, dependence of the intensity ratio. References 9 and 10 measured this excitation laser energy dependency in the Raman spectra of nanographites, and the ratio between the D and G bands was shown to depend on E_L^4.

There is, however, a fundamental geometric difference between defects related to the size of a nanocrystallite and point defects in the sp^2 carbon lattices, resulting in a different intensity ratio dependence on the amount of disorder. Basically, the amount of disorder in a nanocrystallite is given by the amount of border (one-dimensional defects) with respect to the total crystallite area, and this is a measure of L_a. In graphene with zero-dimensional pointlike defects, the distance between defects, L_D, is a measure of the amount of disorder, and recent experiments show that different approaches must be used to quantify L_D and L_a by Raman spectroscopy.[28] The effect of changing L_D on peak width, frequency, intensity, and integrated area for many Raman peaks in single layer graphene was studied in ref 29 and extended to few layer graphene in ref 30 all using a single laser line E_L = 2.41 eV.

Here, to fully accomplish the protocol for quantifying pointlike defects in graphene using Raman spectroscopy (or equivalently, L_D), we use different excitation laser lines in ion-bombarded samples and measure the D to G peak intensity ratio. This ratio is denoted in literature as I_D/I_G or I(D)/I(G), while the corresponding area ratio, i.e., frequency integrated intensity ratio, as A_D/A_G or A(D)/A(G). In principle, for small disorder or perturbations, one should always consider the area ratio, since the area under each peak represents the probability of the whole
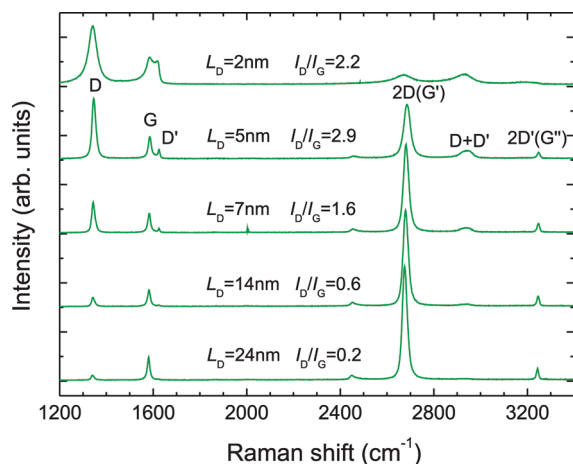
Figure 1. Raman spectra of five ion bombarded SLG measured at E_L =2.41 eV (λ_L =514.5 nm). The L_D are independently measured following the procedure of ref 28 and outlined in the main text. The main Raman peaks are labeled. The respective I_D/I_G values are indicated for each spectrum. The notation within parentheses [e.g., 2D(G′)] indicate two commonly used notations for the same peak (2D and G′).[31,43]

process, considering uncertainty.[29,36] However, for large disorder it is far more informative to decouple the information on peak intensity and full width at half-maximum. The latter, denoted in literature as FWHM or Γ, is a measure of structural disorder,[10,22,29] while the intensity represents the phonon modes/molecular vibrations involved in the most resonant Raman processes.[18,19,22] For this reason, in this paper we will consider the decoupled I_D/I_G and peak widths trends. We find that, for a given L_D, I_D/I_G increases as the excitation laser energy increases. We present a set of empirical formulas that can be used to quantify the amount of pointlike defects in graphene samples with $L_D \geq$ 10 nm using any excitation laser energy/wavelength in the visible range. The analysis of the D and G peak widths and their dispersions with excitation energy unambiguously discriminate between the two main stages of disordering incurred by such samples. We note that, by definition, our analysis only applies to defects able to activate the D peak in the Raman process. For example, it is well-known that perfect zigzag edges do not give rise to a D peak,[32,33] so a set of samples with an increasing amount of ideal zigzag edges would have a constant D peak, determined by other defects.

We produce single layer graphene (SLG) samples with increasing defect density by mechanical exfoliation followed by Ar^+-bombardment, as for the procedure outlined in ref 28. The ion-bombardment experiments are carried out in an OMICRON VT-STM ultrahigh vacuum system (base pressure 5×10^{-11} mbar) equipped with an ISE 5 Ion Source. The Ar^+ ions have 90eV kinetic energy and form an incidence angle of 45° with respect to the normal direction of the sample's surface. According to theoretical calculations, single and double vacancies in the graphene lattice are produced under these conditions.[37,38] Raman spectra are measured at room temperature with a Renishaw microspectrometer. The spot size is ~1 μm for a 100× objective, and the power is kept at ~1.0 mW to avoid heating. The excitation energies, E_L, (wavelengths, λ_L) are Ti−Sapph 1.58 eV (785 nm), He−Ne 1.96 eV (632.8 nm), and Ar^+ 2.41 eV (514.5 nm).

Figure 1 plots the Raman spectra of five SLG samples exposed to different ion bombardment doses in the range 10^{11} Ar^+/cm^2 (one defect per 4×10^4 C atoms) to 10^{15} Ar^+/cm^2 (one defect for every four C atoms). The bombardment procedure described in ref 28 is accurately reproducible. By tuning the bombardment exposure, we generated samples with L_D = 24, 14, 13, 7, 5, and 2 nm. All spectra in Figure 1 are taken at E_L =2.41 eV (λ_L =514.5 nm).

The Raman spectra in Figure 1 consist of a set of distinct peaks. The G and D appear around 1580 and 1350 cm^{-1}, respectively. The G peak corresponds to the E_{2g} phonon at the Brillouin zone center. The D peak is due to the breathing modes of six-atom rings and requires a defect for its activation.[4,18,19,39] It comes from transverse optical (TO) phonons around the $\mathbf{K}$ or $\mathbf{K}'$ points in the first Brillouin zone,[4,18,19] involves an intervalley double resonance process,[39,40] and is strongly dispersive[41] with excitation energy due to a Kohn Anomaly at $\mathbf{K}$.[42] Double resonance can also happen as intravalley process, i.e., connecting two points belonging to the same cone around $\mathbf{K}$ or $\mathbf{K}'$.[40] This gives the so-called D′ peak, which is centered at ~1620 cm^{-1} in defective samples measured at 514.5 nm.[12] The 2D peak (also called G′ in the literature) is the second order of the D peak.[12,31] This is a single peak in single layer graphene, whereas it splits in four in bilayer graphene, reflecting the evolution of the electron band structure.[31,43] The 2D′ peak (also called G″ in analogy to G′) is the second order of D′. Since 2D(G′) and 2D′(G″) originate from a process where momentum conservation is satisfied by two phonons with opposite wavevectors, no defects are required for their activation, and are thus always present. On the other hand, the D + D′ band (~ 2940 cm^{-1}) is the combination of phonons with different momenta, around $\mathbf{K}$ and Γ, thus requires a defect for its activation.

Reference 18 proposed a three stage[44] classification of disorder to simply assess the Raman spectra of carbons along an amorphization trajectory leading from graphite to tetrahedral amorphous carbon: (1) graphite to nanocrystalline graphite; (2) nanocrystalline graphite to low sp^3 amorphous carbon; (3) low sp^3 amorphous carbon to high sp^3 (tetrahedral) amorphous carbon. In the study of graphene, stages 1 and 2 are the most relevant and are summarized here.

In stage 1, the Raman spectrum evolves as follows:[18,28,29] (a) D appears and I_D/I_G increases; (b) D′ appears; (c) all peaks broaden. In the case of graphite the D and 2D lose their doublet structure;[18,46] (e) D + D′ appears; (f) at the end of stage 1, G and D′ are so wide that they start to overlap. If a single Lorentzian is used to fit G and D′, this results in an upshifted wide G band at ~1600 cm^{-1}.

In stage 2, the Raman spectrum evolves as follows:[18] (a) the G peak position, denoted in the literature as Pos(G) or ω_G, decreases from ~1600 cm^{-1} toward ~1510 cm^{-1}; (b) the Tuinstra and Koenig relation fails and I_D/I_G decreases toward 0; (c) ω_G becomes dispersive with the excitation laser energy, the dispersion increasing with disorder; (d) there are no more well-defined second-order peaks, but a broad feature from ~2300 to ~3200 cm^{-1} modulated by the 2D, D + D′, and 2D′ bands.[18,29]

In disordered carbons ω_G increases as the excitation wavelength decreases from IR to UV.[18] The dispersion rate, Disp(G) = $\Delta\omega_G/\Delta E_L$, increases with disorder. The G dispersion separates carbon materials into two types. In those with only sp^2 rings, Disp(G) saturates at ~1600 cm^{-1}, the G position at the end of stage 1. In contrast, for those containing sp^2 chains (such as in amorphous and diamondlike carbons), G continues to rise past
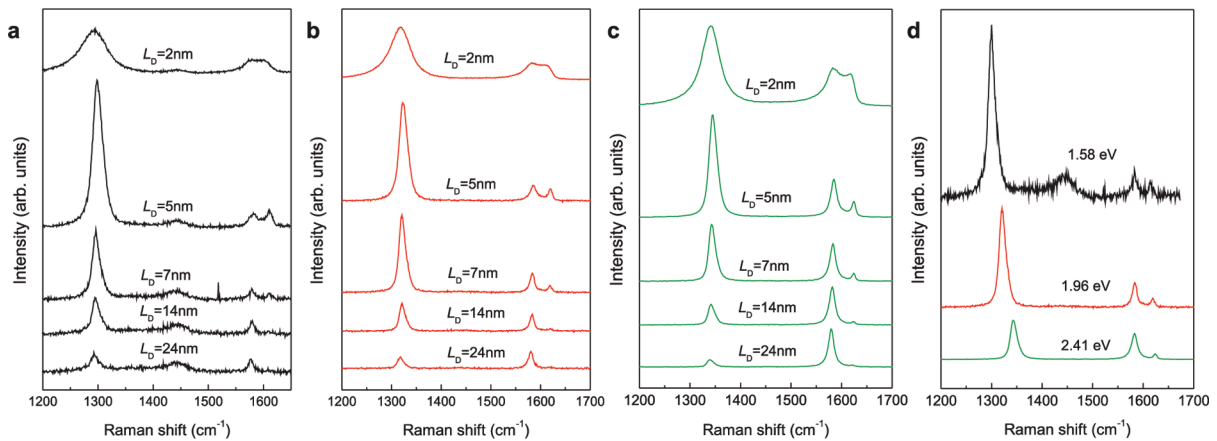
Figure 2. (a−c) Raman spectra of five ion-bombarded SLGs measured with E_L =1.58 eV (λ_L =785 nm), E_L =1.96 eV (λ_L =632.8 nm), and E_L =2.41 eV (λ_L =514.5 nm), respectively. (d) Raman spectra of an ion-bombarded SLG with L_D = 7 nm obtained using these three excitation energies. The band ~1450 cm^{-1} in the Raman spectra at 785nm is a third-order peak of the silicon substrate.[33,47]

1600 cm^{-1} and can reach ~1690 cm^{-1} for 229 nm excitation.[18,19] On the other hand, D always disperses with excitation energy.[18,19] Γ_G always increases with disorder.[10,24,28,29] Thus, combining I_D/I_G and Γ_G allows one to discriminate between stages 1 or 2, since samples in stage 1 and 2 could have the same I_D/I_G, but not the same Γ_G, this being much bigger in stage 2.[24,28,29]

We note that Figure 1 shows the loss of sharp second order features in the Raman spectrum obtained from the L_D = 2 nm SLG. This is an evidence that the range of defect densities in our study covers stage 1 (samples with L_D = 24, 14, 13, 7, 5 nm) and the onset of stage 2 (sample with L_D = 2 nm).

Figure 2a−c reports the first-order Raman spectra of our ion-bombarded SLGs measured at E_L =1.58 eV (λ_L =785 nm), 1.96 eV (632.8 nm), and 2.41 eV (514.5 nm), respectively. Figure 2d shows the Raman spectra of the ion-bombarded SLG with L_D = 7 nm obtained using the three different laser energies. We note that I_D/I_G changes considerably with the excitation energy. This is a well-known effect in the Raman scattering of sp^2 carbons.[9,10,18,19,48,49] Reference 10 noted that the integrated areas of different peaks depend differently on excitation energy E_L: while A_D, $A_{D'}$, and A_{2D} shown no E_L-dependence, A_G was found to be proportional to E_L^4. The independence of A_{2D} on E_L agrees with the theoretical prediction[50] if one assumes that the electronic scattering rate is proportional to the energy. However, a fully quantitative theory is not trivial since, in general, A_D depends not only on the concentration of defects, but on their type as well (e.g., only defects able to scatter electrons between the two valleys **K** and **K**' can contribute).[32−34] Different defects can also produce different frequency and polarization dependence of A_D.[32−34]

Figure 3 plots I_D/I_G for all SLGs and laser energies. For all E_L, I_D/I_G increases as L_D decreases (stage 1), reaches a maximum at $L_D \sim 3$ nm, and decreases toward zero for L_D < 3 nm (stage 2). It is important to understand what the maximum of I_D/I_G vs L_D means. I_D will keep increasing until the contribution from each defect sums independently.[28,33] In this regime (stage 1) I_D is proportional to the total number of defects probed by the laser spot. For an average defect distance L_D and laser spot size L_L, there are on average $(L_L/L_D)^2$ defects in the area probed by the laser, thus $I_D \propto (L_L/L_D)^2$. On the other hand, I_G is proportional to
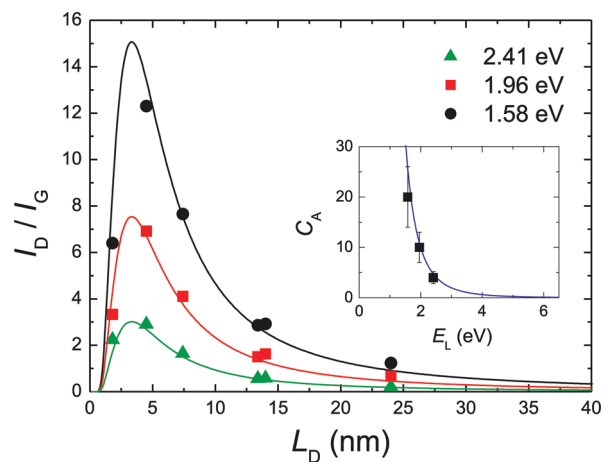
Figure 3. I_D/I_G for all SLGs and laser energies considered here. Solid lines are fits according to eq 1 with r_S = 1 nm and r_A = 3.1 nm. The inset plots C_A as a function of E_L. The solid curve is given by $C_A = 160\ E_L^{-4}$.

the total area probed by the laser ($I_G \propto L_L^2$), giving $I_D/I_G \propto 1/L_D^2$.[18,28] However, if two defects are closer than the average distance an e-h pair travels before scattering with a phonon, then their contributions will not sum independently anymore.[28,29,33,35] This distance can be estimated as $v_F/\omega_D \sim 3$ nm,[33] where $v_F \sim 10^6$ m/s is the Fermi velocity around the **K** and **K**' points, in excellent agreement with the predictions of ref 33 and the data of refs 28, 29, and 35. For an increasing number of defects (stage 2), where L_D < 3 nm, sp^2 domains become smaller and the hexagons in the honeycomb lattice fewer and more distorted, until they open up. As the G peak is just related to the relative motion of sp^2 carbons, we can assume I_G roughly constant as a function of disorder. Thus, with the loss of sp^2 rings, I_D will decrease with respect to I_G and the $I_D/I_G \propto 1/L_D^2$ relation will no longer hold. In this regime, $I_D/I_G \propto M$ (M being the number of ordered hexagons), and the development of a D peak indicates ordering, exactly the opposite to stage 1.[18] This leads to a new relation: $I_D/I_G \propto L_D^2$.[18]

The solid lines in Figure 3 are fitting curves following the relation proposed in ref 28

$$\frac{I_D}{I_G} = C_A \frac{(r_A^2 - r_S^2)}{(r_A^2 - 2r_S^2)} \left[e^{-\pi r_S^2/L_D^2} - e^{-\pi (r_A^2 - r_S^2)/L_D^2} \right] \quad (1)$$

r_A and r_S in eq 1 are length scales that determine the region where the D band scattering takes place. r_S determines the radius of the structurally disordered area caused by the impact of an ion. r_A is defined as the radius of the area surrounding the point defect in which the D band scattering takes place, although the sp^2 hexagonal structure is preserved.[28] In short, the difference $r_A - r_S$ defines the Raman relaxation length of the D band scattering and is associated with the coherence length of electrons that undergo inelastic scattering by optical phonons.[28,35] The fit in Figure 3 is done considering $r_S = 1$ nm (as determined in ref 28 and expected to be a structural parameter, i.e., E_L independent). Furthermore, within experimental accuracy, all data can be fit with the same $r_A = 3.1$ nm, in excellent agreement with the values obtained in refs 28, 29, and 35. Any uncertainty in r_A does not affect the results in the low defect density regime ($L_D > 10$ nm) discussed later.

Reference 28 suggested that I_D/I_G depends on both an activated (A) area, weighted by the parameter C_A, and a structurally defective area (S), weighted by a parameter C_S. Here we selected $C_S = 0$ for two reasons: (i) C_S should be defect-structure dependent, and in the ideal case where the defect is the breakdown of the C−C bonds, C_S should be null; (ii) here we do not focus on the large defect density regime, $L_D < r_S$. The parameter C_A in eq 1 corresponds to the maximum possible I_D/I_G, which would be observed in the ideal situation where the D band would be activated in the entire sample, with no breakdown of any hexagonal carbon ring.[28]

C_A has been addressed in ref 28 as related to the ratio between the scattering efficiency of optical phonons between K and Γ. As we show here, the large I_D/I_G dependence on E_L comes from the change on C_A, which suggests this parameter might also depend on interference effects, when summing the different electron/hole scattering processes that are possible when accounting for the Raman cross section.[51−55] Note that C_A decreases as the laser energy increases. The solid line in the inset to Figure 3 is the fit of the experimental data (dark squares) by using an empirical relation between the maximum value of I_D/I_G and E_L, of the form $C_A = A E_L^{-B}$. The fit yields $A = (160 \pm 48)$ eV^4, by setting $B = 4$ in agreement with refs 9 and 10.

We now focus on the low-defect density regime ($L_D \geq 10$ nm), since this is the case of most interest in order to understand how Raman active defects limit the ultimate mobility of graphene samples.[1−3] In this regime, where $L_D > 2r_A$, the total area contributing to the D band scattering is proportional to the number of point defects, giving rise to $I_D/I_G \propto 1/L_D^2$, as discussed above. For large values of L_D, eq 1 can be approximated to

$$\frac{I_D}{I_G} \simeq C_A \frac{\pi (r_A^2 - r_S^2)}{L_D^2} \quad (2)$$

By taking $r_A = 3.1$ nm, $r_S = 1$ nm, and also the relation $C_A = (160 \pm 48) E_L^{-4}$ obtained from the fit of the experimental data shown in Figure 3, eq 2 can be rewritten as

$$L_D^2 \ (\text{nm}^2) = \frac{(4.3 \pm 1.3) \times 10^3}{E_L^4} \left(\frac{I_D}{I_G} \right)^{-1} \quad (3)$$
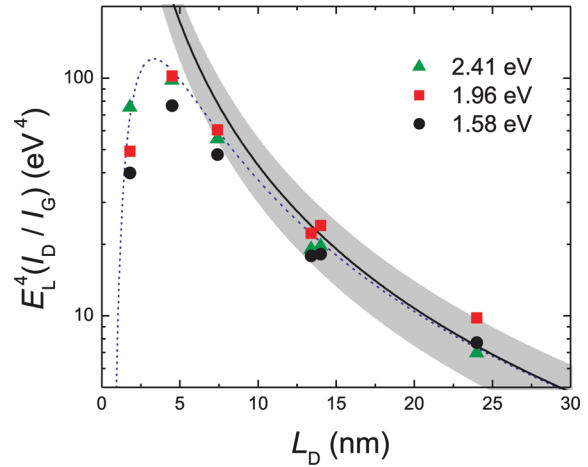
Figure 4. $E_L^4(I_D/I_G)$ as a function of L_D for the data shown in Figure 3. The dashed blue line is the plot obtained from the substitution of the relation $C_A = (160)/E_L^{-4}$ in eq 1. The solid dark line is the plot of the product $E_L^4(I_D/I_G)$ as a function of L_D according to eq 3. The shadow area accounts for the upper and lower limits given by the ±30% experimental error.

In terms of excitation laser wavelength λ_L (in nanometers), we have

$$L_D^2 \ (\text{nm}^2) = (1.8 \pm 0.5) \times 10^{-9} \lambda_L^4 \left(\frac{I_D}{I_G} \right)^{-1} \quad (4)$$

Equations 3 and 4 are valid for Raman data obtained from graphene samples with point defects separated by $L_D \geq 10$ nm using excitation lines in the visible range. In terms of defect density $n_D \ (\text{cm}^{-2}) = 10^{14}/(\pi L_D^2)$, eqs 3 and 4 become

$$n_D \ (\text{cm}^{-2}) = (7.3 \pm 2.2) \times 10^9 E_L^4 \left(\frac{I_D}{I_G} \right) \quad (5)$$

and

$$n_D \ (\text{cm}^{-2}) = \frac{(1.8 \pm 0.5) \times 10^{22}}{\lambda_L^4} \left(\frac{I_D}{I_G} \right) \quad (6)$$

Figure 4 plots $E_L^4(I_D/I_G)$ as a function of L_D for the data shown in Figure 3. The data with $L_D > 10$ nm measured with different laser energies collapse in the same curve. The dashed blue line is the plot obtained from the substitution of the relation $C_A = (160)/E_L^4$ in eq 1. The solid dark line is the plot $E_L^4(I_D/I_G)$ versus L_D according to eqs 3 and 4. The shadow area accounts for the upper and lower limits given by the ±30% experimental error. The plot in Figure 4 validates these relations for samples with $L_D > 10$ nm.

Although these relations are based on the Raman spectra of ion-bombarded samples, they should be valid for other types of point defects (e.g., resonant scatterers, substitutional atoms) in the limit of large L_D, where the nature of the defect should not have a strong influence on the I_D/I_G ratio. Indeed a similar evolution of the Raman spectra can be seen in ref 27. However, eqs 3−6 are of course limited to Raman active defects. For example, perfect zigzag edges,[32−34] charged impurities,[58−60] intercalants,[61] and uniaxial and biaxial strain[62,63] do not generate a D peak. For these types of "silent" defects, other Raman signatures can be used. A perfect zigzag edge does change the
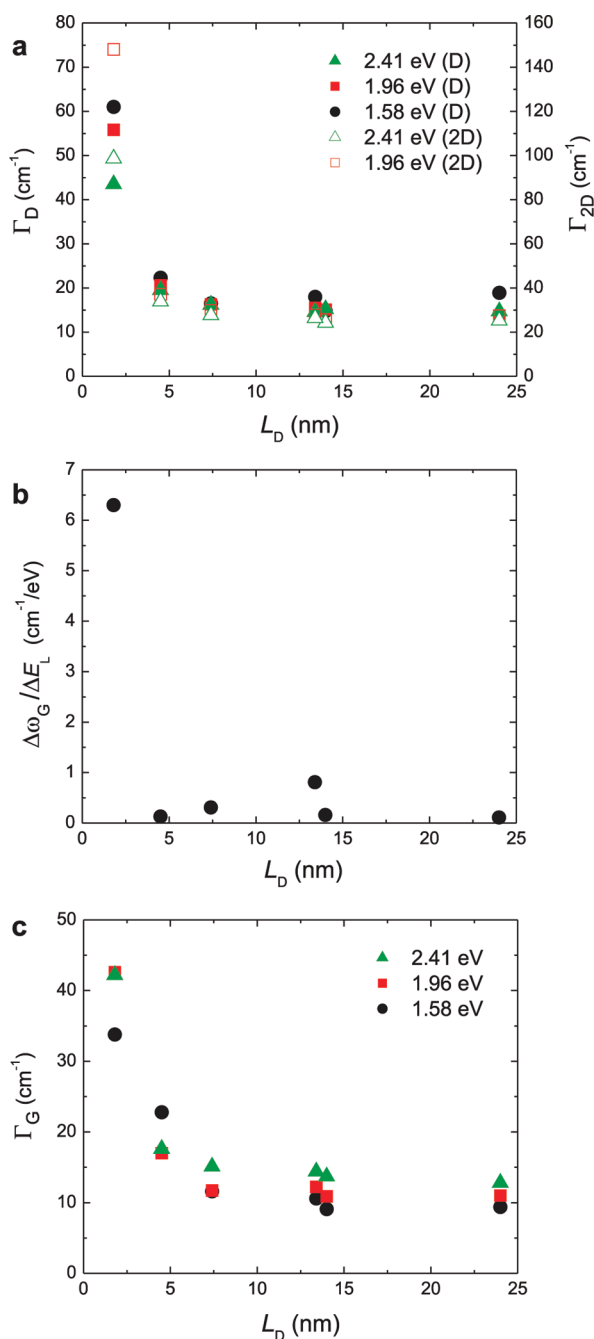
Figure 5. (a) Plot of Γ_D and Γ_{2D} versus L_D. (b) G peak dispersion [Disp(G) = $\Delta\omega_G/\Delta E_L$] as a function of L_D. $\Delta\omega_G/\Delta E_L$ remains zero until the onset of stage 2. (c) FWHM(G) = Γ_G as a function of L_D. As suggested in refs 24 and 29, Γ_G remains roughly constant until the onset of the second stage of amorphization, corresponding to the maximum I_D/I_G.

G peak shape,[64,65] while strain, intercalants, and charged impurities have a strong influence on the G and 2D peaks.[58−62]

Figure 5a plots Γ_D and Γ_{2D} as a function of L_D. Within the experimental error, a dependence of Γ_D or Γ_{2D} on the excitation energy during stage 1 cannot be observed. D and 2D always disperse with excitation energy, with $\Delta\omega_D/\Delta E_L \sim 52$ cm^{-1}/eV, and $\Delta\omega_{2D}/\Delta E_L = 2\Delta\omega_D/\Delta E_L$.

Figures 5b,c plot the G peak dispersion Disp(G) = $\Delta\omega_G/\Delta E_L$ and Γ_G = FWHM(G) as a function of L_D, respectively. As shown

in Figure 5b, $\Delta\omega G/\Delta E_L$ remains zero until the onset of stage two, when it becomes slightly dispersive ($\Delta\omega_G/\Delta E_L \sim 6$ cm^{-1}/ eV). Γ_G (Figure 5c) remains roughly constant at $\sim$14 cm^{-1}, a typical value for as-prepared exfoliated graphene,[11,31,56,57] until the onset of stage 2 (corresponding to the maximum I_D/I_G) as suggested in ref 24 and shown in ref 29 for a single laser line E_L =2.41 eV. Combining I_D/I_G and Γ_G allows to discriminate between stages 1 or 2, since samples in stage 1 and 2 could have the same I_D/I_G, but not the same Γ_G, which is much larger in stage 2.[24,29]

In summary, we discussed the use of Raman spectroscopy to quantify the amount of pointlike defects in graphene. We used different excitation laser lines in ion-bombarded samples in order to measure their respective I_D/I_G. We find that I_D/I_G, for a specific L_D, depends on the laser energy. We presented a set of empirical relations that can be used to quantify point defects in graphene samples with L_D >10 nm via Raman spectroscopy using any laser line in the visible range. We show that the Raman coherence length r_A is E_L-independent, while the strong E_L dependence for I_D/I_G comes from the parameter C_A.[28] By definition, our analysis only applies to defects able to activate the D peak in the Raman process. Some defects do not give rise to the D peak but change other Raman peaks and peaks intensities; other defects are altogether Raman silent. In this case, the combination of Raman spectroscopy with other independent probes of the number of defects in a sample can provide a wealth of information on the nature of such defects.

■ AUTHOR INFORMATION

Corresponding Author
*E-mail: cancado@fisica.ufmg.br.

■ ACKNOWLEDGMENT

■ REFERENCES

(1) Ni, Z.; Ponomarenko, L.; Nair, R; Yang, R.; Anissimova, S.; Grigorieva, I.; Schedin, F.; Blake, P.; Shen, Z.; Hill, E; Novoselov, K. S.; Geim, A. K. On Resonant Scatterers As a Factor Limiting Carrier Mobility in Graphene. *Nano Lett.* **2010**, *10*, 3868–3872.

(2) Chen, J. H.; Cullen, W. G.; Jang, C.; Fuhrer, M. S.; Williams, E. D. Defect scattering in graphene. *Phys. Rev. Lett.* **2008**, *102*, 236805–236808.

(3) Dean, C. R.; Young, A. F.; Meric, I.; Lee, C.; Wang, L.; Sorgenfrei, S.; Watanabe, K.; Taniguchi, T.; Kim, P.; Shepard, K. L.; Hone, J. Boron nitride substrates for high-quality graphene electronics. *Nat. Nanotechnol.* **2010**, *5*, 722–726.

(4) Tuinstra, F.; Koenig, J. L. Raman Spectrum of Graphite. *J. Phys. Chem.* **1970**, *53*, 1126–1130.

(5) Vidano, R.; Fischbach, D. B. New lines in the Raman spectra of carbon and graphite. *J. Am. Ceram. Soc.* **1978**, *61*, 13–17.

(6) Knight, D. S.; White, W. B. Characterization of diamond films by Raman spectroscopy. *J. Mater. Res.* **1989**, *4*, 385–393.

(7) Sinha, K.; Menendez, J. First- and second-order resonant Raman scattering in graphite. *Phys. Rev. B* **1990**, *41*, 10845–10847.

(8) Matthews, M. J.; Pimenta, M. A.; Dresselhaus, G.; Dresselhaus, M. S.; Endo, M. Origin of dispersive effects of the Raman D band in carbon materials. *Phys. Rev. B* **1999**, *59*, R6585–R6588.

(9) Cançado, L. G.; Takai, K.; Enoki, T.; Endo, M.; Kim, Y. A.; Mizusaki, H.; Jorio, A.; Coelho, L. N.; Magalhães-Paniago, R.; Pimenta, M. A. General equation for the determination of the crystallite size L_a of nanographite by Raman spectroscopy. *Appl. Phys. Lett.* **2006**, *88*, 3106–3109.

(10) Cançado, L. G.; Jorio, A.; Pimenta, M. A. Measuring the absolute Raman cross section of nanographites as a function of laser energy and crystallite size. *Phys. Rev. B* **2007**, *76*, 064304–064310.

(11) Ferrari, A. C. Raman spectroscopy of graphene and graphite: Disorder, electron-phonon coupling, doping and nonadiabatic effects. *Solid State Commun.* **2007**, *143*, 47–57.

(12) Nemanich, R. J.; Solim, S. A. First- and second-order Raman scattering from finite-size crystals of graphite. *Phys. Rev. B* **1979**, *20*, 392–401.

(13) Lespade, P.; Marchard, A.; Couzi, M.; Cruege, F. Caracterisation de materiaux carbones par microspectrometrie Raman. *Carbon* **1984**, *22*, 375–385.

(14) Cuesta, A.; Dhamelincourt, P.; Laureyns, J.; Martinez-Alonso, A.; Tascon, J. M. D. Comparative performance of X-ray diffraction and Raman microprobe techniques for the study of carbon materials. *J. Mater. Chem.* **1998**, *8*, 2875–2879.

(15) Wilhem, H.; Lelaurain, M.; McRae, E.; Humbert, B. Raman spectroscopic studies on well-defined carbonaceous materials of strong two-dimensional character. *J. Appl. Phys.* **1998**, *84*, 6552–6558.

(16) Pimenta, M. A.; Dresselhaus, G.; Dresselhaus, M. S.; Cançado, L. G.; Jorio, A.; Saito, R. Studying disorder in graphite-based systems by Raman spectroscopy. *Phys. Chem. Chem. Phys.* **2007**, *9*, 1276–1291.

(17) Zickler, G. A.; Smarsly, B.; Gierlinger, N.; Peterlik, H.; Paris, O. A reconsideration of the relationship between the crystallite size La of carbons determined by X-ray diffraction and Raman spectroscopy. *Carbon* **2006**, *44*, 3239–3246.

(18) Ferrari, A. C.; Robertson, J. Interpretation of Raman spectra of disordered and amorphous carbon. *Phys. Rev. B* **2000**, *61*, 14095–14107.

(19) Ferrari, A. C.; Robertson, J. Resonant Raman spectroscopy of disordered, amorphous, and diamondlike carbon. *Phys. Rev. B* **2001**, *64*, 075414–075426.

(20) Ferrari, A. C.; Robertson, J. (Eds.), Raman spectroscopy in carbons: From nanotubes to diamond. *Philos. Trans. R. Soc., Ser. A* **2004**, *362*, 2267.

(21) Ferrari, A. C.; Robertson, J. Origin of the 1150 cm^{-1} Raman mode in nanocrystalline diamond. *Phys. Rev. B* **2001**, *63*, R121405–R121408.

(22) Casiraghi, C.; Ferrari, A. C.; Robertson, J. Raman spectroscopy of hydrogenated amorphous carbon. *Phys. Rev. B* **2005**, *72*, 085401–085414.

(23) Racine, B.; Ferrari, A. C.; Morrison, N. A.; Hutchings, I.; Milne, W. I.; Robertson, J. Properties of Amorphous Carbon-Silicon Alloys Deposited by A High Plasma Density Source. *J. Appl. Phys.* **2001**, *90*, 5002–5012.

(24) Ferrari, A. C.; Rodil, S. E.; Robertson, J. Interpretation of infrared and Raman spectra of amorphous carbon nitrides. *Phys. Rev. B* **2003**, *67*, 155306–155325.

(25) Hulman, M.; Skakalova, V.; Roth, S.; Kuzmany, H. J. Raman spectroscopy of single-wall carbon nanotubes and graphite irradiated by γ rays. *J. Appl. Phys.* **2005**, *98*, 024311–024315.

(26) Chou, S. G.; Son, H.; Kong, J.; Jorio, A.; Saito, R.; Zheng, M.; Dresselhaus, G.; Dresselhaus, M. S. Length characterization of DNA-wrapped carbon nanotubes using Raman spectroscopy. *Appl. Phys. Lett.* **2007**, *90*, 131109–131111.

(27) Teweldebrhan, D.; Balandin, A. A. Modification of graphene properties due to electron-beam irradiation. *Appl. Phys. Lett.* **2009**, *94*, 013101–013103.

(28) Lucchese, M. M.; Stavale, F.; Ferriera, E. H.; Vilane, C.; Moutinho, M. V. O.; Capaz, R. B.; Achete, C. A.; Jorio, A. Quantifying ion-induced defects and Raman relaxation length in graphene. *Carbon* **2010**, *48*, 1592–1597.

(29) Martins Ferreira, E. H.; Moutinho, M. V. O.; Stavale, F.; Lucchese, M. M.; Capaz, R. B.; Achete, C. A.; Jorio, A. Evolution of the Raman spectra from single-, few-, and many-layer graphene with increasing disorder. *Phys. Rev. B* **2010**, *82*, 125429–125437.

(30) Jorio, A.; Lucchese, M. M.; Stavale, F.; Martins Ferreira, E. H.; Moutinho, M. V. O.; Capaz, R. B.; Achete, C. A. Raman study of ion-induced defects in N-layer graphene. *J. Phys.: Condens. Matter* **2010**, *22*, 334204–334208.

(31) Ferrari, A. C.; Meyer, J. C.; Scardaci, V.; Casiraghi, C.; Lazzeri, M.; Mauri, F.; Piscanec, S.; Jiang, D.; Novoselov, K. S.; Roth, S.; Geim, A. K. Raman Spectrum of Graphene and Graphene Layers. *Phys. Rev. Lett.* **2006**, *97*, 187401–187403.

(32) Cançado, L. G.; Pimenta, M. A.; Neves, B. R. A.; Dantas, M. S. S.; Jorio, A. Influence of the atomic structure on the Raman spectra of graphite edges. *Phys. Rev. Lett.* **2004**, *93*, 247401–247404.

(33) Casiraghi, C.; Hartschuh, A.; Qian, H.; Piscanec, S.; Georgi, C.; Fasoli, A.; Novoselov, K. S.; Basko, D. M.; Ferrari, A. C. Raman Spectroscopy of Graphene Edges. *Nano Lett.* **2009**, *9*, 1433–1441.

(34) Krauss, B.; Nemes-Incze, P.; Skalakova, V; Biro, L. P.; von Klitzing, K.; Smet, J. H. Raman Scattering at Pure Graphene Zigzag Edges. *Nano Lett.* **2010**, *10*, 4544–4548.

(35) Beams, R.; Cançado, L. G.; Novotny, L. Low-Temperature Raman Study of the Electron Coherence Length near Graphene Edges. *Nano Lett.* **2011**, *11*, 1177–1181.

(36) Basko, D. M.; Piscanec, S.; Ferrari, A. C. Electron-electron interactions and doping dependence of the two-phonon Raman intensitym in graphene. *Phys. Rev. B* **2009**, *80*, 165413–165422.

(37) Lehtinen, O; Kotakoski, J.; Krasheninnikov, A. V.; Tolvanen, A.; Nordlund, K.; Keinonen, J. Effects of ion bombardment on a two-dimensional target: Atomistic simulations of graphene irradiation. *Phys. Rev. B* **2010**, *81*, 153401–153404.

(38) Lehtinen, O; Kotakoski, J.; Krasheninnikov, A. V.; Keinonen, J. Cutting and controlled modification of graphene with ion beams. *Nanotechnology* **2011**, *22*, 175306–175313.

(39) Thomsen, C.; Reich, S. Double resonant Raman scattering in graphite. *Phys. Rev. Lett.* **2000**, *85*, 5214–5217.

(40) Saito, R.; Jorio, A.; Souza Filho, A. G.; Dresselhaus, G.; Dresselhaus, M. S.; Pimenta, M. A. Probing phonon dispersion relations of graphite by double resonance Raman scattering. *Phys. Rev. Lett.* **2001**, *88*, 027401–027404.

(41) Vidano, R. P.; Fishbach, D. B.; Willis, L. J.; Loehr, T. M. Observation of Raman band shifting with excitation wavelength for carbons and graphites. *Solid State Commun.* **1981**, *39*, 341–344.

(42) Piscanec, S.; Lazzeri, M.; Mauri, F.; Ferrari, A. C.; Robertson, J. Kohn anomalies and electron-phonon interactions in graphite. *Phys. Rev. Lett.* **2004**, *93*, 185503–185506.

(43) Cançado, L. G.; Reina, A.; Kong, J.; Dresselhaus, M. S. Geometrical approach for the study of G′ band in the Raman spectrum of monolayer graphene, bilayer graphene, and bulk graphite. *Phys. Rev. B* **2008**, *77*, 245408–245416.

(44) Notice that the term "stage" has also been used in graphite intercalation compounds with a different meaning (see ref 45).

(45) Dresselhaus, M. S.; Dresselhaus, G. Intercalation compounds of graphite. *Adv. Phys.* **1981**, *30*, 139–326.

(46) Cançado, L. G.; Takai, K.; Enoki, T.; Endo, M.; Kim, Y. A.; Mizusaki, H.; Speziali, N. L.; Jorio, A.; Pimenta, M. A. Measuring the degree of stacking order in graphite by Raman spectroscopy. *Carbon* **2008**, *46*, 272–275.

(47) Casiraghi, C.; Ferrari, A. C.; Ohr, R.; Chu, D.; Robertson, J. Surface properties of ultra-thin tetrahedral amorphous carbon films for magnetic storage technology. *Diamond Relat. Mater.* **2004**, *13*, 1416–1421.

(48) Pocsik, I.; Hundhausen, M.; Koos, M.; Ley, L. Origin of the D peak in the Raman spectrum of microcrystalline graphite. *J. Non-Cryst. Solids* **1998**, *227–230*, 1083–1086.

(49) Mernagh, T. P.; Cooney, R. P.; Johnson, R. A. Raman spectra of graphon carbon black. *Carbon* **1984**, *22*, 39–42.

(50) Basko, D. M. Theory of resonant multiphonon Raman scattering in graphene. *Phys. Rev. B* **2008**, *78*, 125418–125459.

(51) Maultzsch, J.; Reich, S; Thomsen, C. Double-resonant Raman scattering in graphite: Interference effects, selection rules, and phonon dispersion. *Phys. Rev. B* **2004**, *70*, 155403–155411.

(52) Basko, D. M. Calculation of the Raman G peak intensity in monolayer graphene: role of Ward identities. *New J. Phys.* **2009**, *11*, 095011–095022.

(53) Kalbac, M.; et al. The Influence of Strong Electron and Hole Doping on the Raman Intensity of Chemical Vapor-Deposition Graphene. *ACS Nano* **2010**, *10*, 6055–6063.

(54) Chen, C. F.; Park, C. H.; Boudouris, B. W.; Horng, J; Geng, B; Girit, C.; Zettl, A.; Crommie, M. F.; Segalan, R. A.; Louie, S. G.; Wang, F. Controlling inelastic light scattering quantum pathways in graphene. *Nature* **2011**, *471*, 618–620.

(55) Venezuela, P.; Lazzeri, M.; Mauri, F. *Theory of double-resonant Raman spectra in graphene: intensity and line shape of defect-induced and two-phonon bands*. arXiv:1103.4582 2011.

(56) Pisana, S.; Lazzeri, M.; Casiraghi, C.; Novoselov, K. S.; Geim, A. K.; Ferrari, A. C.; Mauri, F. Breakdown of the adiabatic Born-Oppenheimer approximation in graphene. *Nat. Mater.* **2007**, *6*, 198–201.

(57) Lazzeri, M.; Piscanec, S.; Mauri, F.; Ferrari, A. C.; Robertson, J. Phonon linewidths and electron-phonon coupling in graphite and nanotubes. *Phys. Rev B* **2006**, *73*, 155426–155431.

(58) Casiraghi, C.; Pisana, S.; Novoselov, K. S.; Geim, A. K.; Ferrari, A. C. Raman fingerprint of charged impurities in graphene. *Appl. Phys. Lett.* **2007**, *91*, 233108–233110.

(59) Das, A.; Pisana, S.; Chakraborty, B.; Piscanec, S.; Saha, S. K.; Waghmare, U. V.; Novoselov, K. S.; Krishnamurthy, H. R.; Geim, A. K.; Ferrari, A. C.; Sood, A. K. Monitoring dopants by Raman scattering in an electrochemically top-gated graphene transistor. *Nat. Nanotechnol.* **2008**, *3*, 210–215.

(60) Prado, M. C.; Nascimento, R.; Moura, L. G.; Matos, M. J. S.; Mazzoni, M. S. C.; Cançado, L. G.; Chacham, H.; Neves, B. R. A. Two-Dimensional Molecular Crystals of Phosphonic Acids on Graphene. *ACS Nano* **2010**, *5*, 394–398.

(61) Zhao, W. J.; Tan, P. H.; Liu, K.; Ferrari, A. C. Intercalation of Few-Layer Graphite Flakes with $FeCl_3$: Raman Determination of Fermi Level, Layer by Layer Decoupling, and Stability. *J. Am. Chem. Soc.* **2011**, *133*, 5941–5946.

(62) Mohiuddin, T. M. G.; Lombardo, A.; Nair, R. R.; Bonetti, A.; Savini, G.; Jalil, R.; Bonini, N.; Basko, D. M.; Galiotis, C.; Marzari, N.; Novoselov, K. S.; Geim, A. K.; Ferrari, A. C. Uniaxial strain in graphene by Raman spectroscopy: G peak splitting, Grüneisen parameters, and sample orientation. *Phys. Rev. B* **2009**, *79*, 205433–205440.

(63) Proctor, J. E.; Gregoryanz, E.; Novoselov, K. S.; Lotya, M.; Coleman, J. N.; Halsall, M. P. High-pressure Raman spectroscopy of graphene. *Phys. Rev. B* **2009**, 073408–073411.

(64) Sasaki, K.; Yamamoto, M.; Murakami, S.; Saito, R.; Dresselhaus, M. S.; Takai, K.; Mori, T.; Enoki, T.; Wakabayashi, K. Kohn anomalies in graphene nanoribbons. *Phys. Rev. B* **2009**, *80*, 155450–155460.

(65) Sasaki, K.; Wakabayashi, K.; Enoki, T. Polarization dependence of Raman spectra in strained graphene. *Phys. Rev. B* **2010**, *82*, 205407–205416.